Benchmarking Higher Energy Collision Dissociation (HCD) by Investigation of Binding Energies of Gas-phase Host–Guest Complexes of Hemicryptophane Cages

Parisa Bayat, David Gatineau, Denis Lesage, Alexandre Martinez, Richard Cole

Benchmarking higher energy collision dissociation (HCD) by investigation of binding energies of gas-phase host–guest complexes of hemicryptophane cages

Parisa Bayat[1] | David Gatineau[1,2] | Denis Lesage[1] | Alexandre Martinez[3] | Richard B. Cole[1]

[1]Institut Parisien de Chimie Moléculaire, Sorbonne Université, UMR 8232, CNRS, Paris, France

[2]Département de Chimie Moléculaire, Université Grenoble Alpes, UMR 5250, CNRS, Grenoble, France

[3]Centrale Marseille, iSm2, Aix Marseille Université, CNRS, Marseille, France

Correspondence
Richard B. Cole, Institut Parisien de Chimie Moléculaire, Sorbonne Université, UMR 8232, CNRS, Paris 75252, France.
Email: richard.cole@sorbonne-universite.fr

Funding information
Arcane Labex, Grant/Award Number: ANR-11-LABX-0003-01; Bourse Ministérielle

Abstract

Synthesis of host molecules that feature well-defined characteristics for molecular recognition of guest molecules is often a major aim of synthetic host–guest (H–G) chemistry. A key consideration in evaluating the selectivity of hosts and the affinities of guests is the measurement of binding energies of obtained H–G complexes. In contrast to nuclear magnetic resonance (NMR) or fluorescence measurements that are capable of measuring binding strengths *in solution*, mass spectrometry offers the opportunity to measure *gas-phase* binding energies. Presented in this article is a higher energy collision dissociation (HCD) approach for determining critical energies of dissociation of H–G complexes. Experiments were performed on electrospray ionization (ESI)-generated H–G pairs in an LTQ-XL/Orbitrap hybrid instrument. The presented HCD approach requires preliminary calibration of the internal energy distribution of generated ions that was achieved by the use of activation parameters that were known from previous low-energy collision-induced dissociation (low-energy CID) experiments. Internal energy deposition was modeled based on a truncated Maxwell–Boltzmann distribution and characteristic temperature (T_{char}). Using this method, critical energies of dissociation were determined for 10 H–G biologically relevant complexes of the heteroditopic hemicryptophane cage host (**Host**). Obtained results are compared with those found previously by low-energy CID. The use of this HCD technique is relatively straightforward, although its implementation does require knowledge (or a presumption) about the Arrhenius pre-exponential factor of the complexes to obtain their critical energies of dissociation.

KEYWORDS
binding energy, HCD, hemicryptophane, host–guest, RRKM modeling

1 | INTRODUCTION

Higher energy collision dissociation (HCD) is a non-resonant excitation mode that takes place in a dedicated octopole collision cell of the LTQ-XL/Orbitrap hybrid instrument.[1] In this cell, precursor ions are excited by the voltage offset between the C-trap and HCD octopole, allowing energy uptake upon collision with N_2 (collision gas) and leading to subsequent decompositions. Afterwards, the product ions and the remaining precursor ions are transferred into the Orbitrap for detection.[1,2] Commonly, for comparison purposes, survival yield (*SY*) is plotted

as a function of energy in the center of mass frame of reference.[3] *SY* curves have sigmoidal shapes, and their inflection points are usually used to compare the relative stabilities of a series of complexes.[4–8]

There are various parameters influencing the position of the *SY* curves such as the number of collisions (which depends on the size of the ion and the target gas pressure), critical energy (E_0), entropy of activation, and available time for decomposition that all combine to determine the "kinetic shift"[9,10] (i.e., the energy excess that needs to be applied to the precursor ion relative to its critical energy of dissociation in order to observe fragmentation in the time scale of mass spectrometric detection). By using energy in the center of mass frame of reference, the effect of the changing mass of the ions can be taken into account. However, there is a need for a means to more thoroughly consider all of the above-mentioned influencing parameters.

The current paper investigates a series of 10 host–guest (H–G) systems, all employing a heteroditopic hemicryptophane cage (**Host**) that serves as host for 10 different biologically relevant guests (Figure 1). Activation energies (E_a) for dissociation of these H–G complexes have been previously investigated using a low-energy collision-induced dissociation (low-energy CID) approach inside the linear ion trap of an LTQ-XL/Orbitrap hybrid instrument.[11] Here, their relative stabilities are studied employing the HCD technique[1] using a previously explained method[12] in which after generation of *SY* curves, Rice–Ramsperger–Kassel–Marcus (RRKM) modeling is performed in order to obtain the critical energies.[13–16] Eventually, the critical energies for dissociation of the H–G complexes obtained using different techniques will be compared.

It is worth noting here that critical energy is the difference of the potential energy between the precursor ion in its ground state and the transition state at 0 K, whereas activation energy is the difference between the internal energy content of the precursor ion and that of the transition state at the temperature of the experiment that is defined only for thermal reactions. The connection between these two quantities can be found elsewhere.[17] Similar to the low-energy CID technique, this approach requires preliminary calibration of the internal energy distribution. This was achieved by the use of a previously studied H–G complex, namely, [**Host** +**1**-H]$^+$, (Figure 1), whose activation parameters were known from low-energy CID experiments.[11]

2 | EXPERIMENTAL SECTION

2.1 | Chemicals

The hemicryptophane cage (**Host**) (Figure 1A) was synthesized according to a previously described procedure,[18] and its stock solution (1 mM) was made using dichloromethane. Stock solutions (1 mM) of betaine (**1**), glycine (**2**), β-alanine (**3**), 4-aminobutyric acid (**4**), 7-aminoheptanoic acid (**5**), and 4-aminobenzoic acid (**7**) were prepared in methanol; the remaining guest molecules (i.e., phenylglycine (**6**), aminomethanesulfonic acid (**8**), taurine (**9**), and 3-amino-1-propanesulfonic acid (**10**)) were prepared as aqueous solutions. Dilution of the host and each guest molecule (1:1) in methanol (to a final concentration of 10^{-6} M for each partner) gave the final individual working solutions.

2.2 | Mass spectrometry

Mass spectrometry experiments were performed using an LTQ-XL/Orbitrap hybrid instrument (Thermo Fisher®, San Jose, CA, USA). Electrospray ionization mass spectrometry (ESI-MS) acquisitions were performed in the positive ion mode using a mass resolving power of 3×10^4 at m/z 400. The average scan number was set at 5, and the maximum ion injection time at 200 ms. The electrospray voltage was set at 3.8 kV, capillary voltage at 50 V, and tube lens offset at 90 V. The drying gas temperature was 275°C, and sheath, auxiliary, and sweep gas flows (all were nitrogen) were set at 35, 0, and 2, respectively (arbitrary units). Solutions were injected into the ion source using a syringe pump at 5 μl/min. For HCD experiments, the precursor ions were isolated with an isolation window width of 3 u in the LTQ. These ions were decomposed in the HCD cell with an activation time of 30 ms using N_2 as collision gas, prior to analysis in the Orbitrap. Laboratory frame-of-reference energy (E_{lab}, varying from 0 to 100 eV) was used (as opposed to normalized energy). A detailed explanation of the HCD decomposition mode of the LTQ/Orbitrap hybrid instrument is presented in a previously published paper.[2]

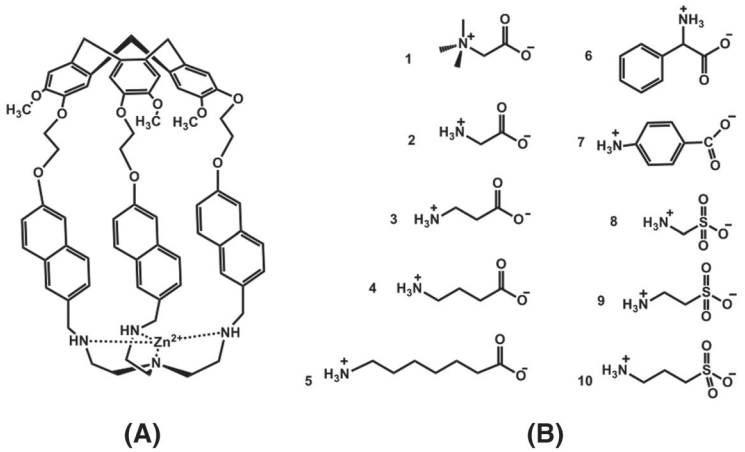

FIGURE 1 (A) Hemicryptophane cage (**Host**) used as host molecule, and (B) guest molecules studied in this work

2.3 | Modeling detail

Kinetic modeling of HCD experiments was performed using *MassKinetics*[19] Scientific Demo software (Version 1.17.2.648 Beta, http://proteomics.ttk.mta.hu/masskinetics/#myPage, generously supplied by Prof. László Drahos). The RRKM formalism was used to undertake computations.[13–16] Calculation of the frequencies of vibrations for precursor ions was performed using the GAMESS[20,21] computational package at the Hartree–Fock level of theory employing a Slater-type basis set. Despite the fact that this level of theory is not high, it has been demonstrated[22,23] that RRKM calculations are not sensitive to the vibrational frequencies when considering only the initial state. A decomposition time of 5 ms[2] was used for simulation of *SY* curves. For this purpose, deposited internal energy and its evolution with time were modeled utilizing a truncated Maxwell–Boltzmann distribution and characteristic temperature (T_{char}). For this simple model, the rate of deactivation is presumed to be negligible, and activation and then fragmentation are considered to be distinct, consecutive steps. Thus, T_{char} corresponds to a thermodynamic temperature reached very rapidly by fast activation processes that take place as a result of multiple collisions, prior to the ions' decomposition.[2,24–26]

From Arrhenius plots obtained previously using low-energy CID experiments[11] (fig. 6 in reference[11]), activation energies (E_a) where experimentally measured. For the purpose of assigning critical energies (E_0) that are required for RRKM modeling of survival yield curves, *MassKinetics*[19] Scientific software (Version 1.17.2.648 Beta) was employed. For computation purposes, ions were considered to remain in thermal equilibrium upon fragmentation. Employing this model, critical energies were fine-tuned until the optimal fit was attained between the experimentally recorded Arrhenius plots and those that were derived computationally.

3 | RESULTS AND DISCUSSION

In order to perform RRKM modeling to extract critical energies from survival yield curves of H–G complexes, the first step is calibration of the deposited internal energy distribution during HCD experiments. Here, we employed the [**Host** +**1**-H]$^+$ complex as a reference complex whose activation parameters were measured using the low-energy CID technique.[11] From previous low-energy CID experiments, the activation energy of the reference H–G complex is known (E_a of 1.66 ± 0.08 eV); however, for calibration of the mean internal energy (<E_{int}>) using RRKM modeling, its critical energy is required. In order to calculate the critical energy, one needs to have a precise description of the transition state. However, for a large system like the [**Host** +**1**-H]$^+$ complex, it is difficult to computationally define the transition state. For this reason, the experimentally measured pre-exponential factor ($log\ A = 15.0\ (\pm 1.1)$)[11] is used in the *MassKinetics* software. Then, considering a thermal system, the critical energy was adjusted in the software until the best fit was attained between the experimentally acquired Arrhenius plot and the computationally obtained one (Figure 2). By doing so, an E_0 of 1.54 eV was found for the reference system.

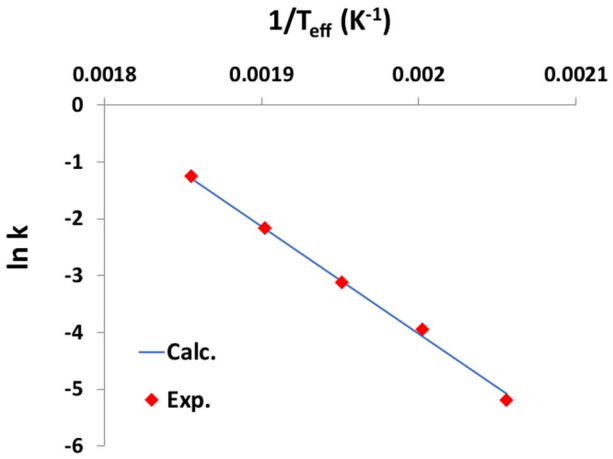

FIGURE 2 Experimentally obtained data points measured using the low-energy collision-induced dissociation (CID) technique, and calculated (line) Arrhenius plots for the dissociation of the [**Host** +**1**-H]$^+$ complex

Afterwards, for HCD measurements, the deposited mean internal energy, <E_{int}>, and corresponding T_{char} for each point of the *SY* curve of the reference complex ([**Host** +**1**-H]$^+$) were obtained using the truncated Maxwell–Boltzmann model. A linear relationship between the energy in the laboratory frame of reference and the mean internal energy was established as follows[2,24–26] (Figure 3):

$$< E_{int} > = 0.1605 \times E_{lab} + 2.464 \quad (1)$$

In Equation 1, the y-intercept of 2.464 eV represents the initial internal energy of the ions before HCD, and this value corresponds to a temperature of 305 K for the reference complex. This initial temperature is not far from the temperature of the N_2 target gas, which is expected to be close to room temperature.[27]

Because all of the H–G pairs under study have very similar structures and numbers of degrees of freedom (DOF), it was presumed that under constant experimental conditions, the amount of energy deposition is almost the same for all H–G complexes in the series. Thus, Equation 1 was used as a reference to gauge the deposited internal energy distribution for all other H–G complexes and was adjusted as follows for the different complexes. In each case, the y-intercept was replaced by the calculated mean internal energy of the chosen H–G complex at the initial temperature of 305 K. This y-intercept, corresponding to initial thermal internal energy, varies with the number of DOF of the studied systems,[28] whereas the slope of Equation 1 was considered to be unchanged.

After calibration of the deposited internal energy, pre-exponential factor values, measured using the low-energy CID resonant excitation approach,[11] were employed to calculate *SY* curves. The critical energy of decomposition for a given H–G

complex was adjusted until the best fit between the experimental and calculated *SY* curves was attained. Obtained critical energies using this approach ($E_{0,HCD}$) are presented in Table 1. Furthermore, guests have been classified based on their functional groups, and then for each class, calculated and experimental *SY* curves are shown in separate plots in Figure 4.

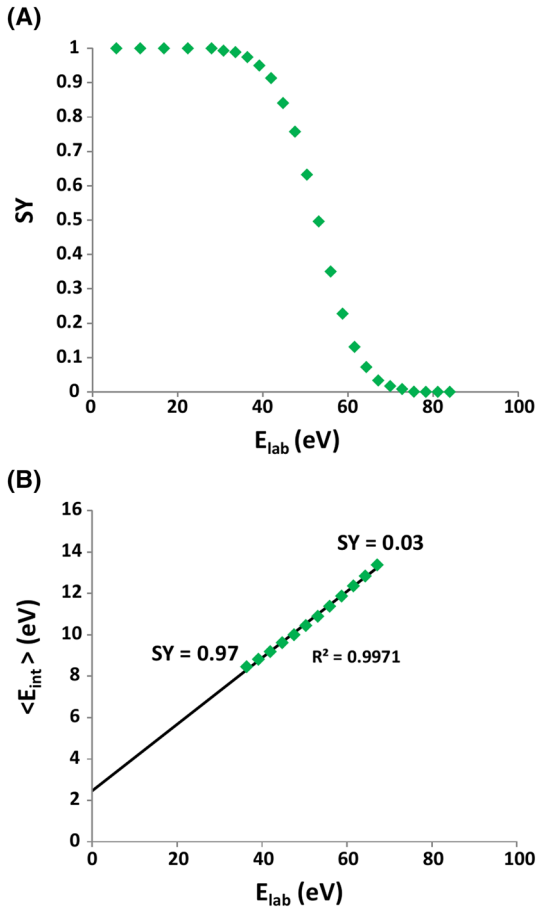

FIGURE 3 (A) Experimental survival yield (*SY*) curve for the dissociation of [**Host** +**1**-H]$^+$ complex in higher energy collision dissociation (HCD) cell. (B) Plot of the calculated mean internal energy versus energy in the laboratory frame of reference

In order to have a direct comparison between the data obtained using the HCD approach and those obtained previously using low-energy CID,[11] an attempt was made to extract critical energies of the H–G complexes from the activation parameters obtained by low-energy CID experiments. For this purpose, by considering a thermal system, RRKM modeling was performed to fit the experimentally obtained Arrhenius plots. This is the same method as was used earlier for simulation of the Arrhenius plot of the reference H–G complex, [**Host** +**1**-H]$^+$, allowing calculation of its critical energy. These calculated critical energies appear in the column labeled "$E_{0,Th}$" in Table 1. For extracting the critical energies from activation parameters, one other method was used, which is based on a previously published article of Laskin and Futrell.[29] In that paper, they have concluded that "Tolman's correction factor (ΔE_{corr}) increases linearly with *log A* from 3 kcal/mol (for *log A* = 16.2) to 36.4 kcal/mol (for *log A* = 39.2)."[29] Here, this linear relation is exploited to calculate Tolman's correction factor for different H–G pairs. Then, critical energies were calculated using Equation 2 at 500 K.[17] Use of this average temperature is appropriate because, under low-energy CID conditions, all of the H–G complexes employed in this study dissociate at effective temperatures between 430 and 580 K. Note that the k_BT term in Equation 2 will vary by only about 0.01 eV over this entire temperature range and ΔE_{corr} will have little temperature dependence for a *log A* value close to 15.[17]

$$E_a = E_0 + \Delta E_{corr} + k_B T \quad (2)$$

These calculated critical energies appear in the column labeled "$E_{0,To}$" in Table 1. To enable visual comparison of the critical energies obtained using the three different techniques, Figure 5 displays results obtained for each H–G complex. From Figure 5, it is evident that $E_{0,To}$ and $E_{0,Th}$ values are very close to each other, and in most cases, both are lower than $E_{0,HCD}$ values. This latter difference may be due to the fact that the same slope was used for the reference H–G complex

H–G pairs	HCD	Low-energy CID		
	$E_{0,HCD}$ (eV)	E_a (eV)	$E_{0,To}$ (eV)	$E_{0,Th}$ (eV)
[**Host** +**1**-H]$^+$	1.54 (±0.08)	1.66 (±0.08)	1.56 (±0.11)	1.54 (±0.08)
[**Host** +**2**-H]$^+$	1.45 (±0.11)	1.45 (±0.10)	1.40 (±0.13)	1.37 (±0.10)
[**Host** +**3**-H]$^+$	1.43 (±0.09)	1.44 (±0.08)	1.39 (±0.11)	1.36 (±0.08)
[**Host** +**4**-H]$^+$	1.42 (±0.10)	1.47 (±0.09)	1.41 (±0.12)	1.38 (±0.09)
[**Host** +**5**-H]$^+$	1.39 (±0.09)	1.51 (±0.08)	1.43 (±0.11)	1.41 (±0.08)
[**Host** +**6**-H]$^+$	1.56 (±0.09)	1.66 (±0.08)	1.54 (±0.11)	1.53 (±0.08)
[**Host** +**7**-H]$^+$	1.50 (±0.12)	1.57 (±0.07)	1.50 (±0.13)	1.47 (±0.07)
[**Host** +**8**-H]$^+$	1.49 (±0.15)	1.48 (±0.13)	1.40 (±0.16)	1.38 (±0.13)
[**Host** +**9**-H]$^+$	1.79 (±0.06)	1.79 (±0.06)	1.74 (±0.08)	1.68 (±0.06)
[**Host** +**10**-H]$^+$	1.70 (±0.06)	1.72 (±0.06)	1.70 (±0.08)	1.63 (±0.06)

Abbreviations: CID, collision-induced dissociation; HCD, higher energy collision dissociation; H–G, host–guest.

TABLE 1 Critical energies for dissociation of H–G complexes measured by (1) low-energy CID experiments[11] using (a) a linear relation presented by Laskin and Futrell[29] at 500 K ($E_{0,To}$), and (b) MassKinetics software with presumption of a thermal model ($E_{0,Th}$), and (2) HCD approach ($E_{0,HCD}$)

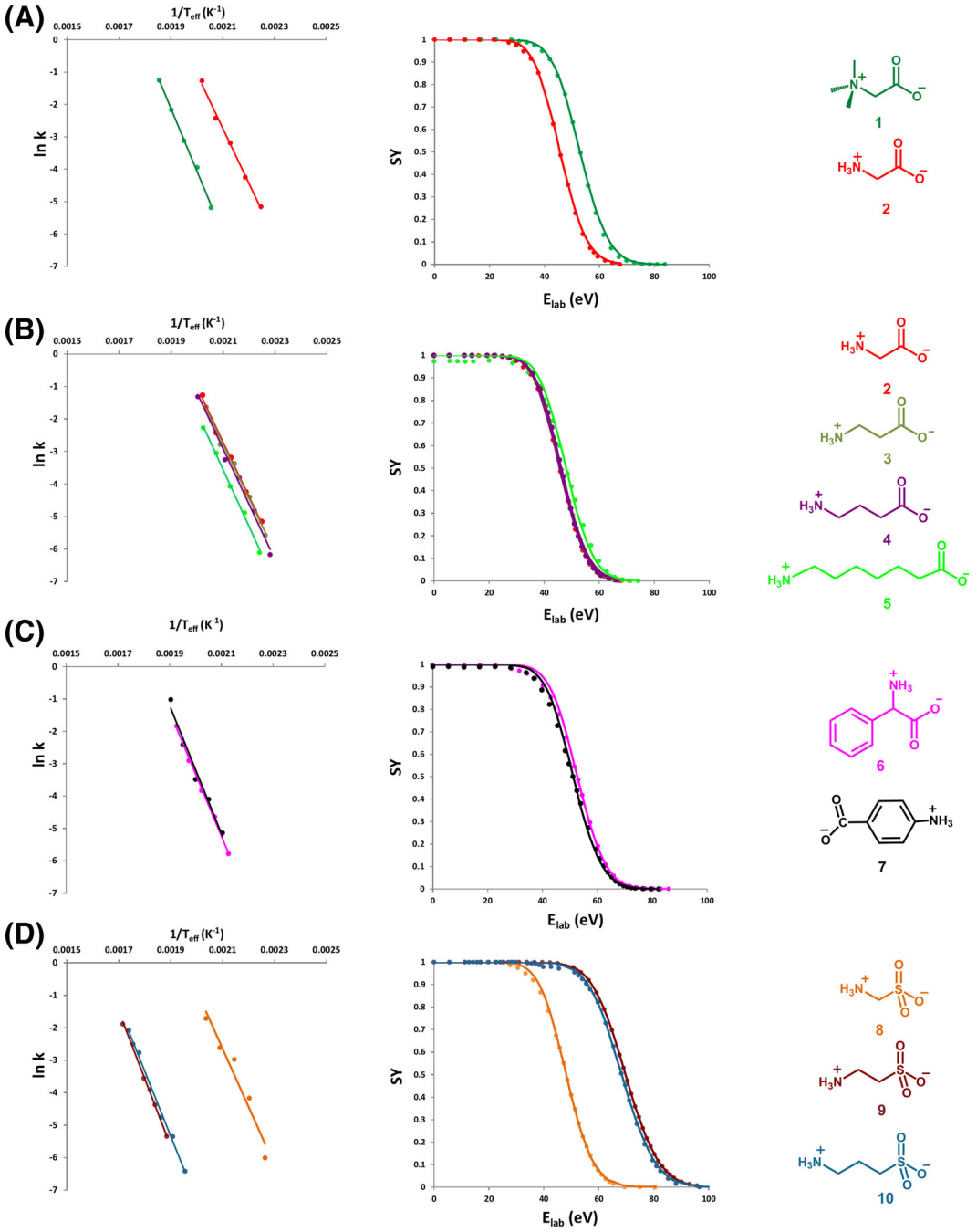

FIGURE 4 (left): Arrhenius plots obtained using low-energy collision-induced dissociation (CID)[11]; (center): experimental (points) and theoretical (lines) for survival yield (*SY*) curves obtained using the higher energy collision dissociation (HCD) approach for the host–guest (H–G) pairs, and classified based on the functional groups present on the guests; (right): (A) compounds 1 and 2; (B) compounds 2–5; (C) compounds 6 and 7; and (D) compounds 8–10

([**Host** +**1-H**]$^+$) and all other H–G pairs in the calibration of mean internal energy in the HCD approach (Equation 1), which can result in uncertainties in $E_{0,HCD}$ values. Nevertheless, the fact that the use of this equation makes it possible to fit the entire set of experimental points constituting the sigmoidal curves, even for the most fragile ([**Host** +**3-H**]$^+$) and for the most sturdy ([**Host** +**9-H**]$^+$) complexes, attests to the validity of this equation; a change in the slope values would not have allowed an acceptable fit for these curves. It should be noted that $E_{0,To}$ and $E_{0,Th}$ values also contain uncertainties. In particular, in the former, an approximate relationship between *log A* and ΔE_{corr} was used for calculation of $E_{0,To}$ values, and in the latter, due to the difficulty in finding the real transition state, experimentally obtained pre-exponential factors (with inherent associated error) were utilized in the procedure for calculation of $E_{0,Th}$ values. Further worth noting is that there are only a few techniques that do not require one to make an estimate or postulation concerning the Arrhenius pre-

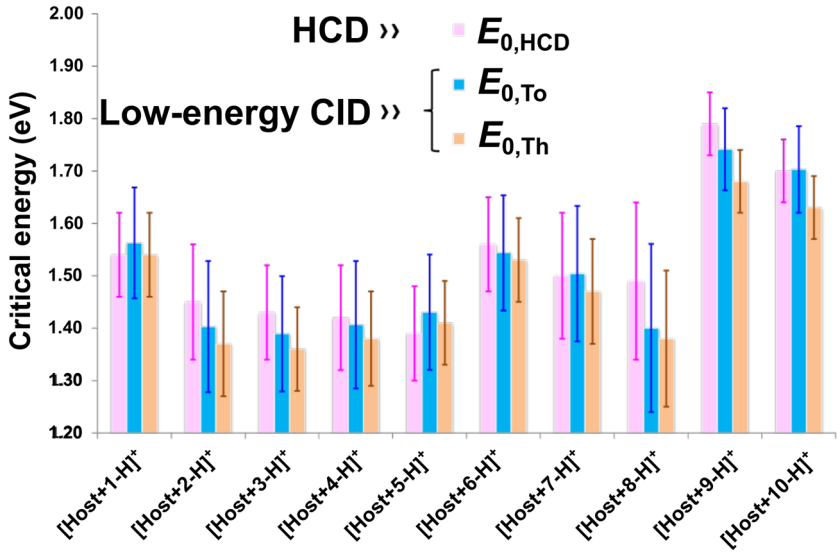

FIGURE 5 Calculated critical energies extracted from (1) low-energy collision-induced dissociation (CID) experiments[11] using (a) a linear relation presented by Laskin and Futrell[29] at 500 K ($E_{0,To}$) and (b) MassKinetics software with presumption of a thermal model ($E_{0,Th}$) and (2) higher energy collision dissociation (HCD) approach ($E_{0,HCD}$)

exponential factor. Examples of techniques that do not require knowledge of the pre-exponential factor are blackbody infrared dissociation (BIRD) (for large systems under rapid exchange [REX] limit conditions),[17,30] low-energy CID (after calibration of effective temperature),[11] threshold photoelectron-photoion coincidence (TPEPICO) spectroscopy,[31] and surface-induced dissociation (SID) on Fourier transform ion cyclotron resonance (FT-ICR).[32] Other robust approaches used to measure E_0 values, such as the threshold collision-induced dissociation (TCID) technique, require either calculations of the transition state frequencies or the assumption that the location of the transition state is at the centrifugal barrier for the products.[31]

3.1 | Comparison of low-energy CID resonant excitation with HCD non-resonant excitation

For investigation of the singly charged H–G complexes, two different techniques were employed to estimate the binding energies of the different guests to the host cage. Both techniques consider that the multiple collision regime leads to Maxwell–Boltzmann internal energy distributions. But on the one hand, low-energy CID is a resonant activation technique in which a lengthy activation time is used (by collision with helium) and where the REX limit[17] is achieved. The precursor ion population may thus be considered to be in thermal equilibrium (at T_{eff}) during all steps of activation and decomposition (Figure 6A). On the other hand, HCD employs non-resonant activation (by collision with nitrogen) where the rate of unimolecular dissociation is much higher than the rate of de-activation of the ions. Therefore, the higher energy tail of the distribution dissociates rapidly, leading to a Maxwell–Boltzmann distribution of internal energy that is truncated on the high-energy end (defined by a T_{char}) (Figure 6B). More details about the different internal energy distribution models commonly used in mass spectrometry such as Maxwell–Boltzmann temperature

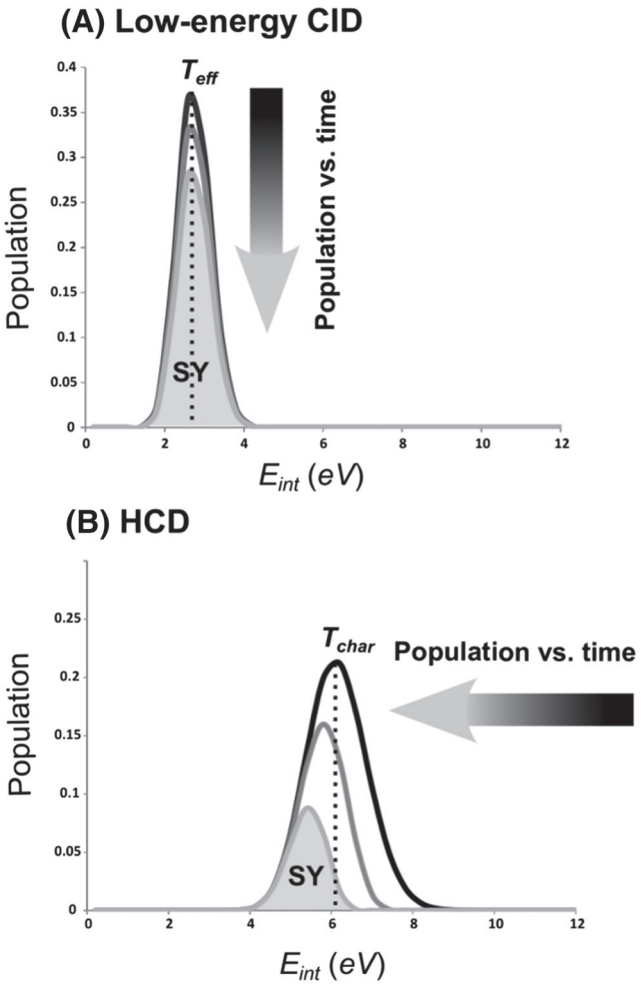

FIGURE 6 Schematic diagrams of (A) thermal model for dissociation of host–guest (H–G) complexes by low-energy collision-induced dissociation (CID) (T_{eff})[17] and (B) truncated Maxwell–Boltzmann distribution for dissociation of H–G complexes (T_{char}) during the higher energy collision dissociation (HCD) process

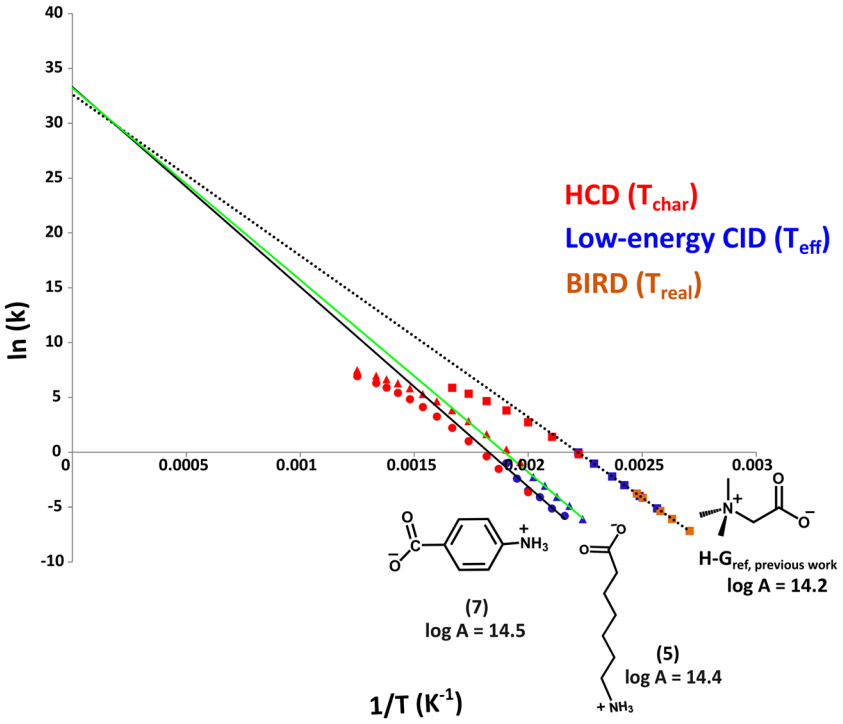

FIGURE 7 Arrhenius plots of H–$G_{ref, previous work}$ (annotated as $[(B+2)+H]^+$) in the previous work,[12] squares), [**Host** +**5**−H]$^+$ (triangles), and [**Host** +**7**−H]$^+$ (circles) obtained using low-energy collision-induced dissociation (CID) (dark blue) and higher energy collision dissociation (HCD) techniques (red). The Arrhenius plot of H–$G_{ref, previous work}$, acquired employing the blackbody infrared dissociation (BIRD) technique (brown) and used as a reference for temperature calibration, is also displayed.

(*T*), characteristic temperature (T_{char}), effective temperature (T_{eff}), and equilibrium truncated thermal Maxwell–Boltzmann internal energy distribution can be found elsewhere.[33,34]

The method of Vékey and co-workers[35] was used to evaluate temperature-dependent rate constants measured using various techniques. Figure 7 presents the Arrhenius plots of three different H–G pairs: reference H–G in our previous work[11] (H–$G_{ref, previous work}$, *log A* = 14.2, structure in Figure S1), [**Host** +**5**-H]$^+$ (*log A* = 14.4), and [**Host** +**7**-H]$^+$ (*log A* = 14.5) obtained using low-energy CID and HCD techniques. The Arrhenius plot of H–$G_{ref, previous work}$ acquired using the BIRD technique[11] is also displayed. BIRD was used to measure activation parameters of the reference complex (H–$G_{ref, previous work}$).[11] An advantage of the BIRD technique is that the real temperatures (T_{real}) of the ions are taken into account and therefore, in contrast to the two other approaches, there is no need for temperature calibration. However, only a relatively low temperature range is accessible (Figure 7), which limits BIRD's application to only systems possessing relatively low dissociation energies.

The second technique included in Figure 7 is low-energy CID, which implicates the effective temperature (T_{eff}) of ions, that is, the temperature corresponding to the Maxwell–Boltzmann distribution of the internal energy of the ions undergoing low-energy CID.[11,36] As is evident from Figure 7, the main advantage of this resonant activation technique is that it enables access to higher temperatures compared with BIRD because the collisional heating inherent to low-energy CID is more efficient than the IR heating used in BIRD to reach an equilibrium temperature under REX limit conditions. Finally, with the third technique, that is, HCD, that encompasses the characteristic temperature of the ions (T_{char}), one can gain access to even higher energy regimes than those of low-energy CID in a shorter activation time. The Arrhenius plot of the H–G pairs acquired using the HCD method (Figure 7) shows that at the beginning of fragmentation, T_{char} is almost equal to T_{eff}. But, at higher dissociation rates, where the internal energy distribution of the precursor ion population starts to become more truncated (at the higher energy portion), T_{char} begins to deviate from T_{eff}. This type of deviation is observed for the BIRD technique when REX limit conditions are not achieved, especially in the case of intermediate-size systems or at high temperatures.[30] This phenomenon is due to a depletion of the high-energy "tail" of the thermal distribution. Under these conditions, the measured activation energy (corresponding to the slope of the line) and the measured natural logarithm of the pre-exponential factor (corresponding to the Y-intercept) exhibit determinate errors to the low side; that is, experimentally determined E_a and ln *A* values are lower than the "true" values.

To obtain the critical energy value when faced with truncation of the high-energy end of the thermal distribution, a complex approach of Master Equation Modeling[30,37] is required. But even with this advanced modeling, the "A" pre-exponential factor is no longer experimentally accessible, and thus, it must be estimated. In the same way, the "A" value cannot be obtained by HCD measurements due to the above-described deviation of the ln k versus 1/*T* plot manifested at higher temperatures.

4 | CONCLUSION

H–G chemistry of the hemicryptophane cage (**Host**) was studied in the gas phase using the HCD fragmentation technique in conjunction with RRKM modeling. Critical energies very similar to those

extracted from low-energy CID experiments were obtained. This technique is straightforward to perform and it can provide reliable results. However, in addition to the requirement for the temperature calibration (as in low-energy CID), the main limitation of this method is that one needs to have information about the pre-exponential factor of the complexes to calculate the critical energies. Therefore, utilization of this technique is only possible when there is some information available concerning the transition state and entropy of dissociation. This HCD investigation into dissociations of hemicryptophane cage H–G complexes complements our previous studies of these same H–G complexes by high-pressure CID[12] and low-energy CID.[11]

REFERENCES

1. Olsen JV, Macek B, Lange O, Makarov A, Horning S, Mann M. Higher-energy C-trap dissociation for peptide modification analysis. *Nat Methods*. 2007;4(9):709-712. doi:10.1038/nmeth1060
2. Ichou F, Schwarzenberg A, Lesage D, et al. Comparison of the activation time effects and the internal energy distributions for the CID, PQD and HCD excitation modes. *J Mass Spectrom*. 2014;49(6):498-508. doi:10.1002/jms.3365
3. Vékey K. Internal energy effects in mass spectrometry. *J Mass Spectrom*. 1996;31(5):445-463. doi:10.1002/(SICI)1096-9888(199605)31:53.0.CO;2-G
4. Wang L, Chai Y, Sun C, Armstrong D. Complexation of cyclofrunctans with transition metal ions studied by electrospray ionization mass spectrometry and collision-induced dissociation. *J Mass Spectrom*. 2012;323–324:21-27. doi:10.1016/j.ijms.2012.06.003
5. Abdoul-carime H, Farizon B, Farizon M, Mulatier J, Dutasta J, Chermette H. Solution vs. gas phase relative stability of the choline/acetylcholine cavitand complexes. *Phys Chem Chem Phys*. 2015;17(6):4448-4457. doi:10.1039/C4CP05354K
6. Kertesz TM, Hall LH, Hill DW, Grant DF. CE50: quantifying collision induced dissociation energy for small molecule characterization and identification. *J Am Soc Mass Spectrom*. 2009;20(9):1759-1767. doi:10.1016/j.jasms.2009.06.002
7. Przybylski C, Bonnet V. Discrimination of cyclic and linear oligosaccharides by tandem mass spectrometry using collision-induced dissociation (CID), pulsed-Q-dissociation (PQD) and the higher-energy C-trap dissociation modes. *Rapid Commun Mass Spectrom*. 2013;27(1):75-87. doi:10.1002/rcm.6422
8. Nagy T, Kuki Á, Antal B, et al. Chiral differentiation of the noscapine and hydrastine stereoisomers by electrospray ionization tandem mass spectrometry. *J Mass Spectrom*. 2015;50(1):240-246. doi:10.1002/jms.3527
9. Lifshitz C. Time-resolved appearance energies, breakdown graphs, and mass spectra: the elusive "kinetic shift". *Mass Spectrom Rev*. 1982;1(4):309-348. doi:10.1002/mas.1280010402
10. Lifshitz C. Kinetic shifts. *Eur J Mass Spectrom*. 2002;8(2):85-98. doi:10.1255/ejms.476
11. Bayat P, Gatineau D, Lesage D, Marhabaie S, Martinez A, Cole RB. Investigation of activation energies for dissociation of host-guest complexes in the gas phase using low-energy collision induced dissociation. *J Mass Spectrom*. 2019;54(5):437-448. doi:10.1002/jms.4345
12. Bayat P, Gatineau D, Lesage D, Robert V, Martinez A, Cole RB. Investigation of hemicryptophane host-guest binding energies using high-pressure collision-induced dissociation in combination with RRKM modeling. *J Am Soc Mass Spectrom*. 2019;30(3):509-518. doi:10.1007/s13361-018-2109-5
13. Rice OK, Ramsperger HC. Theories of unimolecular gas reactions at low pressures. *II J Am Chem Soc*. 1928;50(3):617-620. doi:10.1021/ja01390a002
14. Kassel LS. Studies in homogeneous gas reactions. *I J Phys Chem*. 1928;32(2):225-242. doi:10.1021/j150284a007
15. Marcus RA, Rice OK. The kinetics of the recombination of methyl radicals and iodine atoms. *J Phys Chem*. 1951;55(6):894-908. doi:10.1021/j150489a013
16. Marcus RA. Unimolecular dissociations and free radical recombination reactions. *J Chem Phys*. 1952;20(3):359-364. doi:10.1063/1.1700424
17. Dunbar RC. BIRD (blackbody infrared radiative dissociation): evolution, principles, and applications. *Mass Spectrom Rev*. 2004;23(2):127-158. doi:10.1002/mas.10074
18. Zhang D, Gao G, Guy L, Robert V, Dutasta J-P, Martinez A. A fluorescent heteroditopic hemicryptophane cage for the selective recognition of choline phosphate. *Chem Commun*. 2015;51(13):2679-2682. doi:10.1039/C4CC09428J
19. Drahos L, Vékey K. MassKinetics: a theoretical model of mass spectra incorporating physical processes, reaction kinetics and mathematical descriptions. *J Mass Spectrom*. 2001;36(3):237-263. doi:10.1002/jms.142
20. Schmidt MW, Baldridge KK, Boatz JA, et al. General atomic and molecular electronic structure system. *J Comput Chem*. 1993;14(11):1347-1363. doi:10.1002/jcc.540141112
21. Gordon MS, Schmidt MW. Advances in electronic structure theory: GAMESS a decade later. In: *Theory and Applications of Computational Chemistry: The First Forty Years*. Ames, Iowa: Elsevier B.V.; 2005:1167-1189. doi:10.1016/B978-044451719-7/50084-6.
22. Derrick PJ, Loyd PM, Christie JR. *Physical Chemistry of Ion Reactions in Advanced Mass Spectrometry*. Vol. 13. Chichester, UK: Wiley; 1995.
23. Moon JH, Oh JY, Kim MS. A systematic and efficient method to estimate the vibrational frequencies of linear peptide and protein ions with any amino acid sequence for the calculation of Rice-Ramsperger-Kassel-Marcus rate constant. *J Am Soc Mass Spectrom*. 2006;17(12):1749-1757. doi:10.1016/j.jasms.2006.08.001
24. Naban-Maillet J, Lesage D, Bossée A, et al. Internal energy distribution in electrospray ionization. *J Mass Spectrom*. 2005;40(1):1-8. doi:10.1002/jms.773
25. Pak A, Lesage D, Gimbert Y, Vékey K, Tabet JC. Internal energy distribution of peptides in electrospray ionization: ESI and collision-induced dissociation spectra calculation. *J Mass Spectrom*. 2008;43(4):447-455. doi:10.1002/jms.1330
26. Ichou F, Lesage D, Machuron-Mandard X, Junot C, Cole RB, Tabet J-C. Collision cell pressure effect on CID spectra pattern using triple quadrupole instruments: a RRKM modeling. *J Mass Spectrom*. 2013;48(2):179-186. doi:10.1002/jms.3143
27. Donald WA, Khairallah GN, O'Hair RAJ. The effective temperature of ions stored in a linear quadrupole ion trap mass spectrometer.

J Am Soc Mass Spectrom. 2013;24(6):811-815. doi:10.1007/s13361-013-0625-x

28. Drahos L, Vékey K. Determination of the thermal energy and its distribution in peptides. *J Am Soc Mass Spectrom*. 1999;10(4):323-328. doi:10.1016/S1044-0305(98)00156-1
29. Laskin J, Futrell JH. Entropy is the major driving force for fragmentation of proteins and protein-ligand complexes in the gas phase. *J Phys Chem A*. 2003;107(30):5836-5839. doi:10.1021/jp0345093
30. Price WD, Williams ER. Activation of peptide ions by blackbody radiation: factors that lead to dissociation kinetics in the rapid energy exchange limit. *J Phys Chem A*. 1997;101(47):8844-8852. doi:10.1021/jp9722418
31. Gengeliczki Z, Sztáray B, Baer T, Iceman C, Armentrout PB. Heats of formation of $Co(CO)_2NOPR_3$, R = CH_3 and C_2H_5, and its ionic fragments. *J Am Chem Soc*. 2005;127(26):9393-9402. doi:10.1021/ja0504744
32. Laskin J. Energetics and dynamics of fragmentation of protonated leucine enkephalin from time-and energy-resolved surface-induced dissociation studies. *J Phys Chem A*. 2006;110(27):8554-8562. doi:10.1021/jp057229r
33. Lesage D, Mezzache S, Gimbert Y, Dossmann H, Tabet JC. Extended kinetic method and RRKM modeling to reinvestigate proline's proton affinity and approach the meaning of effective temperature. *Eur J Mass Spectrom*. 2019;25(2):219-228. doi:10.1177/1469066718822054
34. Gatineau D, Dossmann H, Clavier H, et al. Ligand effects in gold-carbonyl complexes: evaluation of the bond dissociation energies using blackbody infrared radiative dissociation. *Int J Mass Spectrom*. 2021;463:116545. doi:10.1016/j.ijms.2021.116545
35. Sztáray J, Memboeuf A, Drahos L, Vékey K. Leucine enkephalin—a mass spectrometry standard. *Mass Spectrom Rev*. 2011;30(2):298-320. doi:10.1002/mas.20279
36. Bayat P, Lesage D, Cole RB. Tutorial: ion activation in tandem mass spectrometry using ultra-high resolution instrumentation. *Mass Spectrom Rev*. 2020;39(5-6):680-702. doi:10.1002/mas.21623
37. Price WD, Schnier PD, Williams ER. Binding energies of the proton-bound amino acid dimers Gly·Gly, Ala·Ala, Gly·Ala, and Lys·Lys measured by blackbody infrared radiative dissociation. *J Phys Chem B*. 1997;101(4):664-673. doi:10.1021/jp9628702